Nanoscale

Accepted Manuscript

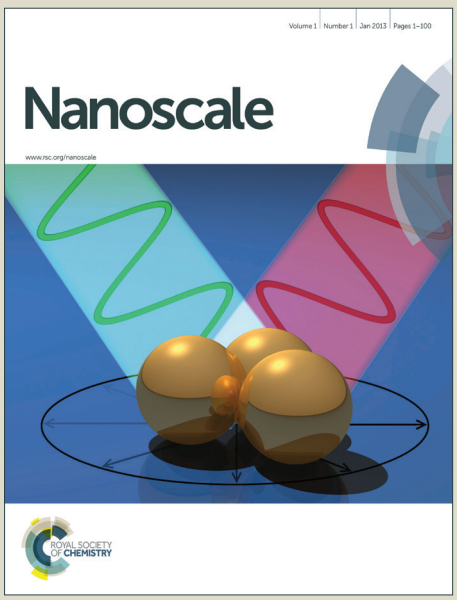

ROYAL SOCIETY OF CHEMISTRY

www.rsc.org/nanoscale

Journal Name

RSCPublishing

ARTICLE

Protein-Based Photothermal Theranostics for Imaging-Guided Cancer Therapy

Cite this: DOI: 10.1039/xoxxoooooox

Pengfei Rong,[a c] Peng Huang,[*b c] Zhiguo Liu,[d] Jing Lin,[e] Albert Jin,[e] Ying Ma,[c] Gang Niu,[c] Lun Yu,[d] Wenbin Zeng,[*d] Wei Wang,[*a] Xiaoyuan Chen[*c]

Received ooth January 2012,
Accepted ooth January 2012

DOI: 10.1039/xoxxoooooox

www.rsc.org/

Development of imageable photothermal theranostics has attracted considerable attention for imaging guided photothermal therapy (PTT) with high tumor ablation accuracy. In this study, we strategically constructed a near-infrared (NIR) cyanine dye by introducing a rigid cyclohexenyl ring to the heptamethine chain to obtain a heptamethine dye CySCOOH with high fluorescence intensity and good stability. By covalent conjugation of CySCOOH onto human serum albumin (HSA), the as-prepared HSA@CySCOOH nanoplatform is highly efficient for NIR fluorescence/photoacoustic/thermal multimodality imaging and photothermal tumor ablation. The theranostic capability of HSA@CySCOOH was systematically evaluated both *in vitro* and *in vivo*. Most intriguingly, complete tumor elimination was achieved by intravenous injection of HSA@CySCOOH (CySCOOH, 1 mg/kg; 808 nm, 1.0 W/cm^2 for 5 min) on 4T1 tumor-bearing mice, with no weight loss, noticeable toxicity, or tumor recurrence being observed. This as-prepared protein-based nanotheranostics exhibits high water dispersibility, no off target cytotoxicity, good biodegradability and biocompatibility, thus facilitating its clinical translation for cancer photothermal theranostics.

Introduction

Proteins, as a class of naturally occurring biomacromolecules, are playing a more and more important role in nanomedicine.[1-4] For example, they have been employed as delivery vehicles for diagnostic/therapeutic agents, and display prolonged blood circulation time to achieve high tumor accumulation rate.[5, 6] They have also been used as coating materials, forming "protein corona" to improve the water-solubility and biocompatibility of nanoparticles.[7-10] Proteins can also serve as bio-templates to direct the *in situ* synthesis of nanoparticles.[11-16] Protein-involved nanotechnology, combining the unique properties and functionalities of both proteins and nanoparticles, promises great potential in clinical translation, as it raises fewer safety concerns than artificially synthesized platforms.[2] As a result, more and more protein-related nanoplatforms, such as an albumin-binding prodrug of doxorubicin (DOX), methotrexate-albumin conjugates, and nanoparticle albumin–bound paclitaxel (PTX) (Abraxane), have been developed for clinical use.[17] Recently, the development of protein-based photothermal theranostics is also an area of great interest.

Photothermal therapy (PTT) has been increasingly recognized as a promising alternative to traditional cancer therapies, such as surgery, radiotherapy, and chemotherapy, due to its spatiotemporal selectivity and minimal invasiveness.[18-25] In the past decade, a series of photothermal theranostics were developed by us and others for simultaneous implementation of bioimaging and PTT.[18, 19] However, many of them contain nonbiodegrable components (e.g. gold and carbon) with potential long-term toxicity, thus have limited clinical use.[17] In order to address the above issues, we recently designed and prepared a novel photothermal theranostics based on near-infrared (NIR) IR820 dye loaded ferritin nanocages with strong NIR absorption for fluorescence/photoacoustic imaging-guided PTT.[17] Wang *et al.* reported the use of squaraine bound bovine serum albumin (BSA) for enhanced fluorescence imaging guided photothermal treatment of cancer.[26] Liu *et al.* used IR825/Indocyanine Green (ICG) dye bound human serum albumin (HSA) with Gd or PTX to form HSA-IR825, HSA-Gd-IR825, and HSA-ICG-PTX for imaging-guided PTT.[27, 28] More recently, Cai group developed HSA-ICG nanoparticles generated by programmed assembly, based on the intermolecular disulfide conjugations within HSA, for dual-modal imaging-guided cancer phototherapy.[29] However, in all these systems, the dyes were bound to the proteins through noncovalent hydrophobic interaction, which results in inevitable dye leakage during blood circulation. In addition, the dye loading efficiency is often too low (for example 1~2 ICG per HSA).[30] Therefore, further development of protein-based photothermal theranostics with improved dye loading and good stability is highly desirable.

Covalent conjugation of dye molecules to protein appears to be

advantageous when compared to the dye encapsulation strategy in constructing protein-based photothermal theranostics, such as good stability without the risk of dye leakage in the blood circulation and high dye loading efficiency. In this study, we strategically designed a NIR cyanine dye by introducing a rigid cyclohexenyl ring to the heptamethine chain to obtain a heptamethine dye CySCOOH with higher fluorescence quantum yield and greater stability than ICG. Meanwhile, we selected HSA, the most prominent protein in human blood plasma, as the dye vehicle. The as-prepared HSA@CySCOOH conjugates were then successfully applied for NIR fluorescence/photoacoustic/thermal multimodality imaging guided PTT.

Results and Discussion

ICG is the only NIR dye approved by the Food and Drug Administration (FDA).[31] It has been used as a clinical cardiac and hepatic blood flow reporter, and as a NIR fluorescence imaging contrast agent of retinal and choroidal vasculature for several decades.[32] However, several drawbacks limit its biomedical application: aqueous-instability, rapid elimination from the liver and bile excretion, and low fluorescence quantum yield due to self-aggregation and photobleaching.[33, 34] To improve the stability and fluorescence quantum yield of ICG, we designed a rigid cyclohexenyl ring in the heptamethine chain to obtain a heptamethine dye CySCOOH. The synthesis route of CySCOOH is shown in **Fig. S1**. The rigid cyclohexenyl ring in the heptamethine chain could improve dye stability, and decrease photobleaching.[35] The CySCOOH covalently bound to the amine groups of the lysine residues within the HSA through a modified EDC-NHS reaction (**Fig. 1a**). To optimize the number of CySCOOH within the HSA@CySCOOH, variable amounts of CySCOOH (2:1, 4:1, 12:1 reaction ratio per HSA) were used in the conjugation reaction. The conjugation efficiency of CySCOOH was calculated by using a CySCOOH calibration curve at 819 nm. The standard curve had a good linear relationship, described by the following equation: Y = 0.13267 X - 0.07244 (R^2 = 0.996). As shown in **Table S1**, HSA@CySCOOH-2, HSA@CySCOOH-4, and HSA@CySCOOH-12 demonstrated 45%, 43% and 34% conjugation efficiency, respectively. There were about 4.1 of CySCOOH per HSA for HSA@CySCOOH-12, which was also evidenced by the LC/MS analysis (**Fig. S2**). HSA@CySCOOH-12 was used for all further studies.

The size and morphology of the HSA@CySCOOH were characterized by atomic force microscopy (AFM) (**Fig. S3** and **Fig. 1b**). Both HSA and HSA@CySCOOH have a well-defined spherical structure with an average size change from 7.3 ± 1.7 to 8.5 ± 1.9 nm (**Fig. 1c**). The size increase of ~1.2 nm can be attributed to the CySCOOH conjugation. The hydrodynamic diameter of HSA@CySCOOH is 38.8 ± 11.1 nm. The zeta potential of HSA@CySCOOH is 0.1 mV. The natural structure conformation of HSA is critical to maintain its biological behaviors such as prolonged blood circulation time. The structure conformations of HSA and HSA@CySCOOH were investigated using a circular dichroism (CD) spectropolarimeter (**Fig. 1d**). Pure HSA showed a positive absorption band at 190 nm and two negative absorption bands at 209 and 222 nm.[12] After conjugation with CySCOOH, the HSA@CySCOOH also showed identical bands, which suggests that the dye conjugation procedure does not substantially change the natural structure conformation of HSA carrier.

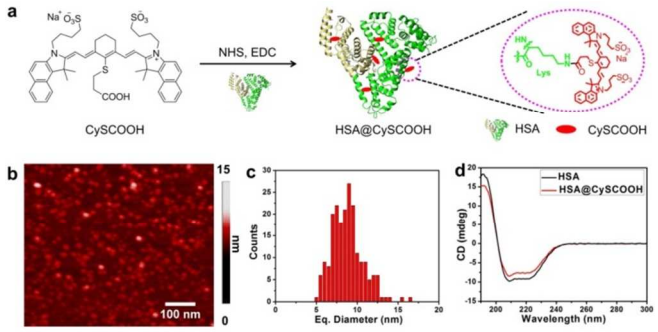

Fig. 1. Synthesis and characterization of HSA@CySCOOH. (a) Synthetic procedure. (b) AFM image. (c) Histogram distribution of the equivalent spherical (Eq.) diameter (Eq. diameter = $(6V/\pi)^{1/3}$). (d) CD spectra of pure HSA and HSA@CySCOOH.

We next investigated the photochemical and photophysical properties of HSA@CySCOOH. **Fig. 2a** shows the UV-Vis-NIR absorbance spectra of HSA (black), CySCOOH (blue), and HSA@CySCOOH (red). HSA exhibits a characteristic absorbance peak at ~280 nm, which is attributed to the π→π* transition of the aromatic amino acid residues such as tyrosine, tryptophan, and phenylalanine.[11] The CySCOOH dye displays a weak shoulder at 744 nm, and a strong peak at 820 nm. HSA@CySCOOH reveals the superimposed peaks of both CySCOOH and HSA, indicating that CySCOOH molecules retained their spectroscopic property after being conjugated.

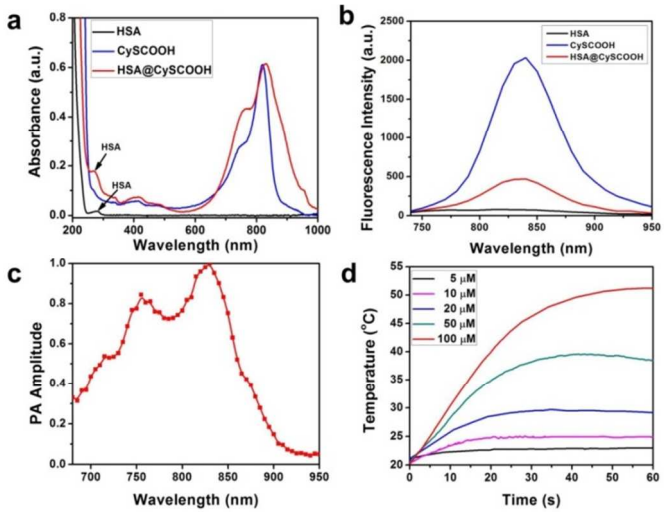

Fig. 2 UV-Vis-NIR (a) and fluorescence emission (b) spectra of HSA (black), CySCOOH (blue), and HSA@CySCOOH (red). (c) Photoacoustic (PA) spectrum of HSA@CySCOOH. (d) Temperature change curves of HSA@CySCOOH solutions exposed to an 808 nm laser at a power density of 1.0 W/cm^2.

As shown in **Fig. 2b**, both CySCOOH and HSA@CySCOOH showed the same fluorescence emission peak at 840 nm, making them highly suitable for NIR fluorescence imaging with deeper tissue penetration and minimal background autofluorescence interference. The observable fluorescence quenching (~77%) could

be ascribed to the dynamic quenching or self-aggregation of CySCOOH molecules after being conjugated to HSA, which will benefit improved photothermal conversion efficiency for PTT.[17] The PA response of HSA@CySCOOH was investigated using an excitation wavelength range of 680 to 950 nm (**Fig. 2c**). The best excitation wavelength was found to be in the range of 750 to 850 nm. To allow both PAI and PTT at the same time, we chose 808 nm as the excitation wavelength for PAI. The photothermal efficiency of HSA@CySCOOH was evaluated by measuring the temperature elevation of the HSA@CySCOOH aqueous solution after being exposed to an 808 nm laser (1 W/cm^2, 1 min) (**Fig. 2d**). HSA@CySCOOH displayed CySCOOH concentration dependent temperature increase.

The cytotoxicity of HSA@CySCOOH (CySCOOH, 12.5~200 μg/mL) was studied on 4T1 cancer cells by measuring their relative cell viabilities after 48 h incubation through MTT assay. Cell viability was normalized to the control group without any treatment. The cell viabilities were more than 95% at all the test concentrations, which suggests that HSA@CySCOOH alone has negligible toxicity to 4T1 cells. Afterwards, the *in vitro* PTT effects of HSA, CySCOOH, and HSA@CySCOOH were studied on 4T1 cells at the same conditions with increasing laser power. For the HSA group, no PTT effect was observed at any of the laser power density applied. Both CySCOOH and HSA@CySCOOH exhibited a laser dose-dependent cytotoxicity to 4T1 cells. Interestingly, HSA@CySCOOH showed much higher PTT efficacy than CySCOOH dye under the same conditions. These results were further verified using live/dead cell staining. Without laser irradiation, cells all displayed green fluorescence, which suggested that either CySCOOH or HSA@CySCOOH alone cannot kill cells. Upon laser irradiation, more cells treated with HSA@CySCOOH were killed compared to the cells in the CySCOOH treated group, as observed by the intensity of red fluorescence (**Fig. 3a**). The results indicated that the *in vitro* PTT effect of HSA@CySCOOH is much higher than that of CySCOOH (**Fig. 3b**), which is in accordance with the MTT assay.

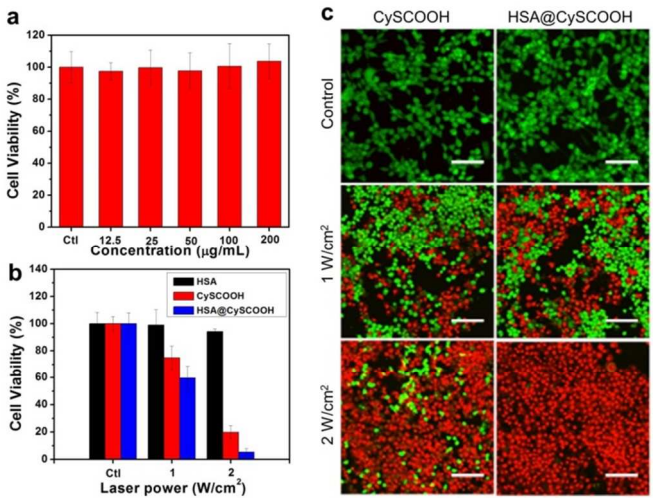

Fig. 3. *In vitro* cell experiments. (a) Cell cytotoxicity of HSA@CySCOOH on 4T1 cells after 48 h incubation. (b) 4T1 cells viabilities at different laser power irradiation for 3 min with 808 nm laser for HSA, HSA@CySCOOH, and CySCOOH. (c) Fluorescence images of Calcein AM and Ethidium homodimer-1 co-stained 4T1 cells incubated with CySCOOH or HSA@CySCOOH for 12 h at different treatments. Scale bars: 50 μm. The data are shown as mean ± SD (n = 3).

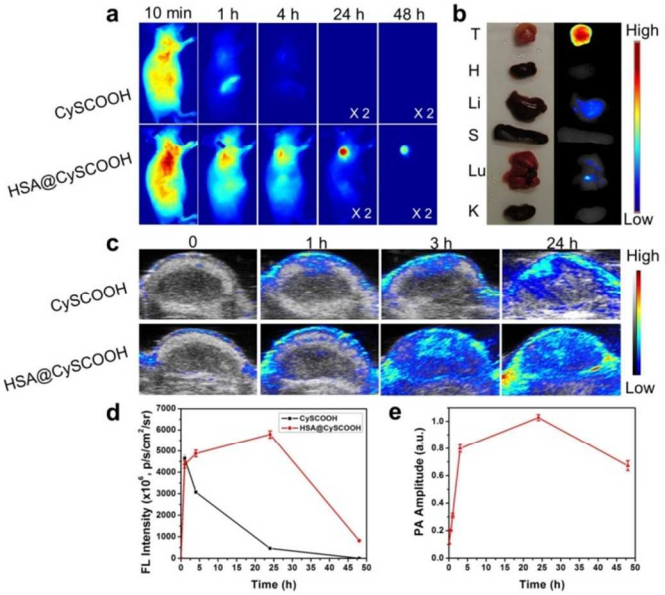

Fig. 4. *In vivo* NIR fluorescence (FL) and PA imaging. (a) *In vivo* NIR FL images of 4T1 tumor-bearing mice after intravenous injection of CySCOOH or HSA@CySCOOH. (b) *Ex vivo* NIR FL image of mouse tissues (from top to bottom: tumor, heart, liver, spleen, lung, kidneys), harvested after 48 h intravenous injection of HSA@CySCOOH. (c) *In vivo* PA images of 4T1 tumor-bearing mice after intravenous injection of CySCOOH or HSA@CySCOOH. (d) Tumor fluorescent intensity of time post-administration of CySCOOH and HSA@CySCOOH. (e) Average PA intensity of tumor tissues at preinjection and postinjection of HSA@CySCOOH. The data are shown as mean ± SD (n = 3).

Encouraged by the photochemical and photophysical properties of HSA@CySCOOH, NIR fluorescence (FL) and PA imaging were employed to monitor the pharmacokinetics of HSA@CySCOOH *in vivo*. Athymic nude mice with subcutaneous 4T1 cancer xenografts were selected as the animal model. When the size of the tumors reached ~100 mm^3, the mice were intravenously injected with CySCOOH (CySCOOH, 1 mg/kg) or HSA@CySCOOH (CySCOOH, 1 mg/kg; HSA, 20 mg/kg), respectively. **Fig. 4a** shows the *in vivo* NIR FL images of 4T1 tumor-bearing mice after intravenous injection of CySCOOH or HSA@CySCOOH at different time points. At 10 min p.i., all mice exhibited fluorescence distributed throughout the whole body. With time, the fluorescence signal of whole body gradually decreased for mice with CySCOOH administration, with a major portion of the CySCOOH being quickly taken up by spleen within 1 h, and excreted within 24 h. In contrast, the mice with HSA@CySCOOH administration exhibited a decrease in the fluorescence signal of the whole body and a continual increase in the tumor site. The tumor can be clearly differentiated from the surrounding normal tissue with good contrast from 1 to 48 h p.i.. Even at 48 h p.i., the tumors still sustained a relatively strong fluorescence signal, which was further evidenced by *ex vivo* NIR FL image (**Fig. 4b**). Meanwhile, PAI was used to observe the PA signal change in the tumor tissue. The continual increase of PA signal was observed in the tumor region of HSA@CySCOOH treated mice,

while negligible PA signal for CySCOOH treated mice was observed (**Fig. 4c**).

The tumor accumulation of CySCOOH or HSA@CySCOOH was compared through the quantification of CySCOOH fluorescence intensity, recorded as total photons per centimeter squared per steradian ($\times 10^6$, p/s/cm^2/sr)(**Fig. 4d**).[36] For HSA@CySCOOH treated mice, the average fluorescence intensity of tumor tissue gradually increased within 0~24 h, followed by a slight decrease over time. In contrast, for CySCOOH treated mice, the average fluorescence intensity of tumor tissue quickly arose within 0~1 h, and dramatically fell within 24 h. Semi-quantification of PA signals in the tumor area also revealed that the average tumor PA intensity continually increased within 0~24 h followed by a slight decrease over time (**Fig. 4e**).These results suggested that HSA carrier can significantly improve tumor accumulation of the CySCOOH molecules.

Based on the observations from FL and PA imaging, both FL and PA signals peak at 24 h p.i., which suggests the highest tumor accumulation of HSA@CySCOOH at that time point. Therefore, the best time for PTT implementation was selected to be at 24 h p.i. of HSA@CySCOOH. HSA and CySCOOH were selected as controls. The tumors were irradiated using a continuous wave laser (808 nm, 1.0 W/cm^2 for 5 min), and the temperature changes were recorded by an infrared (IR) thermal camera. No obvious temperature rise was observed in the HSA treated mice. Both CySCOOH and HSA@CySCOOH treated groups had an obvious tendency to heat up, arriving at maximum temperatures of 43.24 ± 1.09 and 56.27 ± 1.34 ^{o}C, respectively. No significant temperature rise was observed in other parts of the body for both groups. Based on the same laser irradiation condition, the tumor temperature of HSA@CySCOOH group elevated higher than that of CySCOOH group, which promises a better PTT therapeutic efficacy of HSA@CySCOOH than that of CySCOOH.

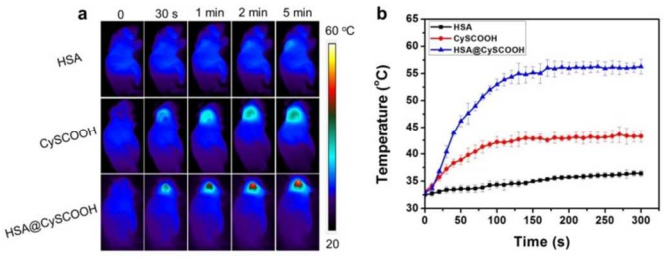

Fig. 5. *In vivo* photothermal imaging. (a) Thermal images of 4T1 tumor-bearing mice exposed to 808 nm laser (1.0 W/cm^2) for 5 min at 24 h postinjection of HSA, CySCOOH or HSA@CySCOOH. (b) Heating curves of tumors upon laser irradiation as a function of irradiation time. The data are shown as mean ± SD (n = 3).

In vivo HSA@CySCOOH-induced PTT treatment was systematically evaluated on 4T1 tumor-bearing mice. Six groups (4-6 mice/group) were designated as follows: mice with HSA administration (HSA, n=4), mice with CySCOOH administration (CySCOOH, n=6), mice with HSA@CySCOOH administration (HSA@CySCOOH, n=5), mice with HSA administration and laser irradiation (HSA + laser, n=6), mice with CySCOOH administration and laser irradiation (CySCOOH + laser, n=5), and mice with

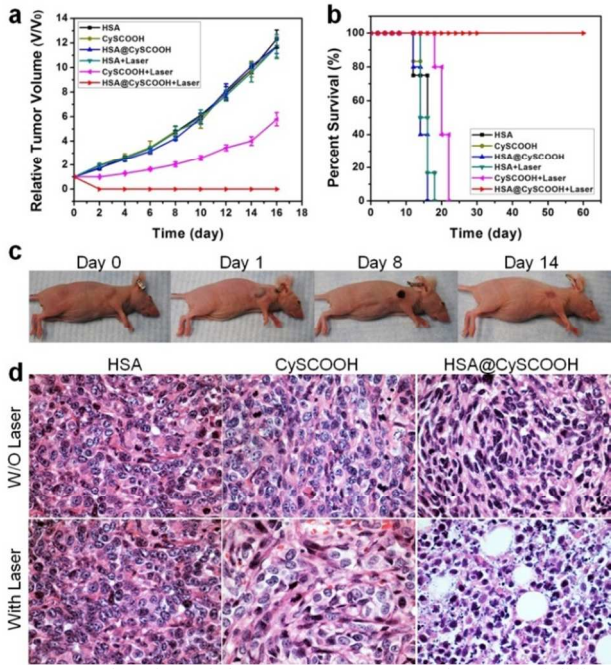

Fig. 6. *In vivo* photothermal therapy. (a) Tumor growth curves of different groups of 4T1 tumor-bearing mice after treatment. Tumor volumes were normalized to their initial sizes. Error bars represent the standard deviation of 4–6 mice per group. (b) Survival curves of 4T1 tumor after bearing mice with various treatments. (c) Representative photographs of 4T1 tumor-bearing mice at different days after HSA@CySCOOH treatment. (d) H&E stained tumor sections collected from different groups of 4T1 bearing mice at 24 h after photothermal therapy.

HSA@CySCOOH administration and laser irradiation (HSA@CySCOOH + laser, n=6). For laser irradiation groups, the tumors were irradiated at 24 p.i. using a continuous wave laser (808 nm, 1.0 W/cm^2 for 5 min). All the tumors that did not undergo laser irradiation displayed similar rapid tumor growth, which indicated negligible therapeutic effects without laser irradiation (**Fig. 6a**). A remarkable delay in tumor growth or tumor regression was observed in both CySCOOH/laser and HSA@CySCOOH/laser groups within 16 days. No tumor reoccurrence was observed with the HSA@CySCOOH/laser treated group, in which all the tumors were effectively ablated, leaving scars at their original sites (**Fig. 6c**). Importantly, mice in the HSA/laser and other no laser treated groups showed average life spans of ~18 days, while all the mice in the CySCOOH/laser group had to be sacrificed on day 22 due to the extensive tumor burden. Interestingly, however, mice in the HSA@CySCOOH/laser treated group were tumor-free after treatment and survived over 60 days without a single death or tumor reoccurrence (**Fig. 6b**), further demonstrating the excellent PTT efficacy of HSA@CySCOOH *in vivo*. The *in vivo* PTT effects were also evidenced by Hematoxylin and eosin (H&E) staining of tumor sections, which were harvested at 2 h after laser irradiation. Significant cancer cell damage with nuclear membrane fragmentation and nuclei shrinkage was only observed in HSA@CySCOOH/laser treated group (**Fig. 6d**). To evaluate the *in vivo* biosafety of HSA@CySCOOH, main organs from different treated groups of mice were observed, and as seen through H&E stained images (**Fig. S5**), showed no obvious damage or

inflammation. This indicates that HSA@CySCOOH has no cytotoxicity and no discernable toxic side effects to treated animals. No significant body weight loss was noted in any of the groups (**Fig. S6**). Although much work is needed to systematically study the potential short-term and long-term toxicity of HSA@CySCOOH at various doses with more animals used per group, our pilot small-scale toxicity study promises further explorations of using HSA protein-based nanomaterials for *in vivo* cancer theranostics.

Experimental Section

Materials: All chemicals were purchased from Sigma-Aldrich Chemical Co. and used without further purification. Calcium acetoxymethyl ester (calcein AM), and ethidium homodimer 1 (EthD-1) were obtained from Invitrogen Corp. (Carlsbad, CA). All chemicals and reagents were of analytical grade. Water was purified with a Milli-Q plus system (Millipore Co., Bedford, MA).

Synthesis of HSA@CySCOOH

The CySCOOH-NHS ester was synthesized by reacting CySCOOH (200 mg, 0.32 mmol, the synthesis of CySCOOH was described in supporting information, **Fig. S1**) with N-hydroxysuccinimide (NHS) (44 mg, 0.38 mmol) in the presence of DCC (65 mg, 0.32 mmol).

After stirring overnight, the reaction mixture was concentrated in vacuum, purified by column chromatography (1:9, MeOH/DCM) and lyophilized to yield CySCOOH-NHS (159 mg, 70%). HSA (5 mg, 75 nmol) was dissolved in a 10 mM phosphate buffer (pH 8.5; 0.5 mL) and 2, 4, or 12 eq. of CySCOOH-NHS (15 mM in DMSO) was added. After 30 min, the reaction mixture was concentrated and washed over a centrifugal filter (Amicon Ultra 50K). The obtained purified HSA@CySCOOH samples were re-dispersed into 1 mL PBS for further characterization and application.

Characterization of HSA@CySCOOH

The size and morphology of HSA@CySCOOH was investigated by atomic force microscopy (AFM). After suitable sample absorption on freshly peeled mica substrate, rinsing, drying, and dehumidification, biological AFM imaging of the HSA or HSA@CySCOOH samples was carried out in air, using gentle tapping-mode AFM with a PicoForce Multimode AFM (Bruker, CA) consisting of a Nanoscope® V controller, a type E scanner head, and a sharpened TESP-SS (Bruker, CA) or similar AFM cantilever. AFM images were evaluated within the Nanoscope software (ver. 7.3-8.15, Bruker, CA) and exported to Image J (ver. 1.4x, National Institutes of Health, MD) for further analyses and display.

UV/Vis spectra were measured by a Genesys 10S UV-Vis spectrophotometer (Thermo Scientific, Waltham, MA) using quartz cuvettes with an optical path of 1 cm. Fluorescence intensity was monitored with an F-7000 fluorescence spectrophotometer (Hitachi, Tokyo, Japan). Thermal images were captured by a SC300 infrared camera (FLIR, Arlington, VA) and processed with Examin IR image software (FLIR). The excitation source was an 808 nm diode-pumped solid-state laser system (LASERGLOW Technologies, Toronto, Canada).

Conjugation efficiency of CySCOOH per HSA

The average number of CySCOOH per HSA was detected by measuring the unconjugated dye in the removed solution after centrifugation-filtration through 50 kDa MWCO Amicon filters. The DMSO/Water (1:9) was chosen as the eluent. The unconjugated dye was calculated by using dye UV calibration curve at 819 nm. The standard curve had a good linear relationship, described by the following typical equation: $Y = 0.13267\ X - 0.07244$ ($R^2 = 0.99594$).

Cell culture

MTT assays were used to measure cellular viability. Human breast cancer MCF-7 cells were seeded at a density of 5000 cells/well in 96-well plates for 24 h, and then incubated with free Dox, MSN-Dox MSN-Dox@GO or MSN-Dox@GO-Apt (The equivalent Dox concentrations are 0.1, 0.2, 0.4, 0.8 and 1.6 μg/mL, respectively) for another 24 h. The standard MTT assay was carried out to evaluate the cell viability. Five replicates were done for each group. 4T1 cell line was obtained from the American Type Culture Collection (ATCC, Manassas, VA). 4T1 cells were cultured in RPMI-1640 medium supplemented with 10% FBS (GIBCO, Grand Island, NY) and 1% penicillin/streptomycin (100 mg/mL) solution at 37°C and 5% CO_2.

Cell toxicity assay

4T1 cells were seeded in 96-well cell culture plates at a density of 1×10^4 per well for 24 h and then fed with CySCOOH, or HSA@CySCOOH (CySCOOH, 12.5~200 μg/mL) for another 48 h. Afterwards, the standard MTT assay was carried out to evaluate the cell viability.

***In vitro* photothermal therapy**

4T1 cells were seeded in 96-well plates at a density of 5×10^3 cells/well in RPMI-1640 complete medium, and grown to 60-80% confluence. The cells were incubated with HSA, free CySCOOH, or HSA@CySCOOH at the same CySCOOH concentration of 100 μM for 24 h. The wells were then washed three times with PBS. Fresh medium (100 μl) was added into cells, which were immediately irradiated by the 808 nm laser at various laser powers (1.0 and 2.0 W/cm^2) for 10 min. The plates were returned to the incubator for further cultivation overnight. Cell viability was estimated by the standard MTT assay.

Animal model

Athymic nude mice were obtained from Harlan laboratories (Frederick, USA) under protocols approved by National Institutes of Health Clinical Center Animal Care and Use Committee (CC/ACUC). The 4T1 tumor mice were generated by subcutaneous injection of 1×10^6 cells in 200 μl of PBS into the right shoulder of nude mice. The mice were used for imaging and PTT when the tumor volume reached ~100 mm^3.

***In vivo* NIR fluorescence/photoacoustic imaging**

When the tumor size reached ~100 mm^3, the 4T1 tumor-bearing mice were intravenously (i.v.) injected with CySCOOH (CySCOOH, 1 mg/kg) or HSA@CySCOOH (CySCOOH, 1 mg/kg; HSA, 20 mg/kg). Fluorescence imaging was performed with a Maestro all-optical imaging system (Caliper Life Sciences, Hopkinton, MA) at 10 min, 1 h, 4 h, 24 h, and 48 h post-injection. The CySCOOH spectrum was unmixed from autofluorescence by Maestro 2 software (Caliper Life Sciences). PA imaging was performed using a Vevo 2100 LAZR system (VisualSonics Inc. New York, NY) equipped with a 40 MHz, 256-element linear array transducer on tumors.

***In vivo* photothermal therapy**

When the tumor size reached ~100 mm^3, 4T1 tumor-bearing mice

were divided into 6 groups: mice with HSA administration (HSA, n=4); mice with CySCOOH administration (CySCOOH, n=6); mice with HSA@CySCOOH administration (HSA@CySCOOH, n=5); mice with HSA administration and laser irradiation (HSA + laser, n=6); mice with CySCOOH administration and laser irradiation (CySCOOH + laser, n=5), and mice with HSA@CySCOOH administration and laser irradiation (HSA@CySCOOH + Laser, n=6). The injection dose was HSA (20 mg/kg), CySCOOH (CySCOOH, 1 mg/kg), and HSA@CySCOOH (CySCOOH, 1 mg/kg; HSA, 20 mg/kg). For the laser irradiation groups, the tumors were irradiated at 24 post-injection (p.i.) using continuous wave laser (808 nm, 1.0 W/cm^2 for 5 min). Mice were monitored for 60 days post-treatment. The tumor volume (V) was calculated by the following equation: $V = A*B^2/2$, where A is the longer diameter and B is the shorter diameter (mm). The relative tumor volumes were normalized to their initial sizes. Mice were euthanized for ethical consideration when the tumor volume reached 2000 mm^3. On the other hand, mice were considered cured if there was no palpable tumor by day 60. The tumor weights were measured every other day.

***Ex vivo* histological staining**

Major organs were dissected from different groups of euthanized 4T1 tumor-bearing mice. Tissues were fixed in 4% formaldehyde solution at room temperature. Haematoxylin and eosin (H&E) staining (BBC Biochemical, Mount Vernon, WA) was performed following the manufacturer's instructions and observed by a BX41 bright-field microscopy (Olympus).

Conclusions

In summary, we successfully developed an imageable photothermal theranostics platform based on a heptamethine dye, CySCOOH conjugated HSA (HSA@CySCOOH), for NIR fluorescence/photoacoustic/thermal multimodality imaging and photothermal tumor ablation. The covalent bond between CySCOOH and HSA avoids the risk of dye leakage into blood circulation, and also improves dye loading. More importantly, the HSA carrier can prolong the blood circulation time of CySCOOH, and improve tumor accumulation efficiency of CySCOOH *via* the enhanced permeability and retention (EPR) effect over free CySCOOH. We further validated the strong photothermal effect of HSA@ CySCOOH both *in vitro* and *in vivo*. NIR fluorescence and photoacoustic imaging was used to monitor the pharmacokinetics of HSA@CySCOOH *in vivo*, and guide the PTT treatment. Complete tumor elimination was achieved by intravenous injection of HSA@CySCOOH with low laser irradiation dose (808 nm, 1.0 W/cm^2 for 5 min). Our results indicated that the as-prepared protein-based nanotheranostics have potential for clinical translation for cancer photothermal theranostics.

Acknowledgements

This work was supported by the Intramural Research Program (IRP) of the National Institute of Biomedical Imaging and Bioengineering (NIBIB), National Institutes of Health (NIH), and grants from National Natural Science Foundation of China (81401465, 81471715, 30900359, 30900377 and 81271634), Doctoral Station of Ministry of Education of China (No. 20120162110070), Hunan Provincial Natural Science Foundation of China (12JJ1012).

Notes

[a] *Department of Radiology, the Third Xiangya Hospital, Central South University, Changsha, 410013, PR China*

[b] *Department of Biomedical Engineering, School of Medicine, Shenzhen University, Guangdong Key Laboratory for Biomedical Measurements and Ultrasound Imaging, Shenzhen, China, 518060*

[c] *Laboratory of Molecular Imaging and Nanomedicine (LOMIN), National Institute of Biomedical Imaging and Bioengineering (NIBIB), National Institutes of Health (NIH), Bethesda, Maryland 20892, United States*

[d] *School of Pharmaceutical Sciences, Central South University, Changsha, 410013, PR China*

[e] *Laboratory of Cellular Imaging and Macromolecular Biophysics, National Institute of Biomedical Imaging and Bioengineering (NIBIB), National Institutes of Health (NIH), Bethesda, Maryland 20892, United States*

Corresponding authors: peng.huang@nih.gov (P. Huang); cjr.wangwei@vip.163.com (W. Wang); wbzeng@hotmail.com (W. Zeng); or shawn.chen@nih.gov (X. Chen).

Reference

1 S. Tenzer, D. Docter, J. Kuharev, A. Musyanovych, V. Fetz, R. Hecht, F. Schlenk, D. Fischer, K. Kiouptsi, C. Reinhardt, K. Landfester, H. Schild, M. Maskos, S. K. Knauer and R. H. Stauber, *Nat. Nanotechnol.*, 2013, **8**, 772-781.

2 M. J. Hawkins, P. Soon-Shiong and N. Desai, *Adv. Drug Deliv. Rev.*, 2008, **60**, 876-885.

3 A. Maham, Z. Tang, H. Wu, J. Wang and Y. Lin, *Small*, 2009, **5**, 1706-1721.

4 M. Mahmoudi, I. Lynch, M. R. Ejtehadi, M. P. Monopoli, F. B. Bombelli and S. Laurent, *Chem. Rev.*, 2011, **111**, 5610-5637.

5 Y. Wang, L. Lang, P. Huang, Z. Wang, O. Jacobson, D. O. Kiesewetter, I. U. Ali, G. Teng, G. Niu and X. Chen, *Proc. Natl. Acad. Sci. U. S. A.*, 2015, **112**, 208-213.

6 M. Lundqvist, J. Stigler, G. Elia, I. Lynch, T. Cedervall and K. A. Dawson, *Proc. Natl. Acad. Sci. U. S. A.*, 2008, **105**, 14265-14270.

7 C. D. Walkey and W. C. Chan, *Chem. Soc. Rev.*, 2012, **41**, 2780-2799.

8 I. Lynch, A. Salvati and K. A. Dawson, *Nat. Nanotechnol.*, 2009, **4**, 546-547.

9 P. Aggarwal, J. B. Hall, C. B. McLeland, M. A. Dobrovolskaia and S. E. McNeil, *Adv. Drug Deliv. Rev.*, 2009, **61**, 428-437.

10 A. Salvati, A. S. Pitek, M. P. Monopoli, K. Prapainop, F. B. Bombelli, D. R. Hristov, P. M. Kelly, C. Aberg, E. Mahon and K. A. Dawson, *Nat. Nanotechnol.*, 2013, **8**, 137-143.

11 P. Huang, L. Bao, D. Yang, G. Gao, J. Lin, Z. Li, C. Zhang and D. Cui, *Chem. Asian J.*, 2011, **6**, 1156-1162.

12 H. Hu, P. Huang, O. J. Weiss, X. Yan, X. Yue, M. G. Zhang, Y. Tang, L. Nie, Y. Ma, G. Niu, K. Wu and X. Chen, *Biomaterials*, 2014, **35**, 9868-9876.

13 P. Huang, D. P. Yang, C. Zhang, J. Lin, M. He, L. Bao and D. Cui, *Nanoscale*, 2011, **3**, 3623-3626.

14 P. Huang, Y. Kong, Z. Li, F. Gao and D. Cui, *Nanoscale Res. Lett.*, 2010, **5**, 949-956.

15 J. Lin, Z. Zhou, Z. Li, C. Zhang, X. Wang, K. Wang, G. Gao, P. Huang and D. Cui, *Nanoscale Res. Lett.*, 2013, **8**, 170.

16 P. Huang, J. Lin, S. Wang, Z. Zhou, Z. Li, Z. Wang, C. Zhang, X. Yue, G. Niu, M. Yang, D. Cui and X. Chen, *Biomaterials*, 2013, **34**, 4643-4654.
17 P. Huang, P. Rong, A. Jin, X. Yan, M. G. Zhang, J. Lin, H. Hu, Z. Wang, X. Yue, W. Li, G. Niu, W. Zeng, W. Wang, K. Zhou and X. Chen, *Adv. Mater.*, 2014, **26**, 6401-6408.
18 P. Huang, P. Rong, J. Lin, W. Li, X. Yan, M. G. Zhang, L. Nie, G. Niu, J. Lu, W. Wang and X. Chen, *J. Am. Chem. Soc.*, 2014, **136**, 8307-8313.
19 P. Huang, J. Lin, W. Li, P. Rong, Z. Wang, S. Wang, X. Wang, X. Sun, M. Aronova, G. Niu, R. D. Leapman, Z. Nie and X. Chen, *Angew. Chem. Int. Ed. Engl.*, 2013, **52**, 13958-13964.
20 J. Lin, S. Wang, P. Huang, Z. Wang, S. Chen, G. Niu, W. Li, J. He, D. Cui, G. Lu, X. Chen and Z. Nie, *ACS Nano*, 2013, **7**, 5320-5329.
21 S. Wang, P. Huang, L. Nie, R. Xing, D. Liu, Z. Wang, J. Lin, S. Chen, G. Niu, G. Lu and X. Chen, *Adv. Mater.*, 2013, **25**, 3055-3061.
22 Z. Li, P. Huang, X. Zhang, J. Lin, S. Yang, B. Liu, F. Gao, P. Xi, Q. Ren and D. Cui, *Mol. Pharm.*, 2010, **7**, 94-104.
23 H. Ke, J. Wang, Z. Dai, Y. Jin, E. Qu, Z. Xing, C. Guo, X. Yue and J. Liu, *Angew. Chem. Int. Ed. Engl.*, 2011, **50**, 3017-3021.
24 P. Huang, L. Bao, C. Zhang, J. Lin, T. Luo, D. Yang, M. He, Z. Li, G. Gao, B. Gao, S. Fu and D. Cui, *Biomaterials*, 2011, **32**, 9796-9809.
25 W. Li, P. Rong, K. Yang, P. Huang, K. Sun and X. Chen, *Biomaterials*, 2015, **45**, 18-26.
26 F. P. Gao, Y. X. Lin, L. L. Li, Y. Liu, U. Mayerhoffer, P. Spenst, J. G. Su, J. Y. Li, F. Wurthner and H. Wang, *Biomaterials*, 2014, **35**, 1004-1014.
27 Q. Chen, C. Wang, Z. Zhan, W. He, Z. Cheng, Y. Li and Z. Liu, *Biomaterials*, 2014, **35**, 8206-8214.
28 Q. Chen, C. Liang, X. Wang, J. He, Y. Li and Z. Liu, *Biomaterials*, 2014, **35**, 9355-9362.
29 Z. Sheng, D. Hu, M. Zheng, P. Zhao, H. Liu, D. Gao, P. Gong, G. Gao, P. Zhang, Y. Ma and L. Cai, *ACS Nano*, 2014, **8**, 12310-12322.
30 T. Desmettre, J. M. Devoisselle and S. Mordon, *Surv. Ophthalmol.*, 2000, **45**, 15-27.
31 B. Bahmani, D. Bacon and B. Anvari, *Sci. Rep.*, 2013, **3**, 2180.
32 C. Vinegoni, I. Botnaru, E. Aikawa, M. A. Calfon, Y. Iwamoto, E. J. Folco, V. Ntziachristos, R. Weissleder, P. Libby and F. A. Jaffer, *Sci. Transl. Med.*, 2011, **3**, 84ra45.
33 L. Yan and L. Qiu, *Nanomedicine (Lond)*, 2015, **10**, 361-373.
34 Y. Ma, S. Tong, G. Bao, C. Gao and Z. Dai, *Biomaterials*, 2013, **34**, 7706-7714.
35 C. Zhang, S. Wang, J. Xiao, X. Tan, Y. Zhu, Y. Su, T. Cheng and C. Shi, *Biomaterials*, 2010, **31**, 1911-1917.
36 P. Huang, Z. Li, J. Lin, D. Yang, G. Gao, C. Xu, L. Bao, C. Zhang, K. Wang, H. Song, H. Hu and D. Cui, *Biomaterials*, 2011, **32**, 3447-3458.